Cellular/Molecular

Parvalbumin-Containing Fast-Spiking Basket Cells Generate the Field Potential Oscillations Induced by Cholinergic Receptor Activation in the Hippocampus

Attila I. Gulyás,[1] Gergely G. Szabó,[1] István Ulbert,[2,3] Noémi Holderith,[1] Hannah Monyer,[4] Ferenc Erdélyi,[1] Gábor Szabó,[1] Tamás F. Freund,[1,3] and Norbert Hájos[1]

[1]Institute of Experimental Medicine, Hungarian Academy of Sciences, H-1083, Budapest, Hungary, [2]Institute for Psychology, Hungarian Academy of Sciences, H-1132, Budapest, Hungary, [3]Péter Pázmány Catholic University, Faculty of Information Technology, H-1088, Budapest, Hungary, and [4]Department of Clinical Neurobiology, University Hospital of Neurology, 69120 Heidelberg, Germany

Gamma frequency oscillations in cortical regions can be recorded during cognitive processes, including attention or memory tasks. These oscillations are generated locally as a result of reciprocal interactions between excitatory pyramidal cells and perisomatic inhibitory interneurons. Here, we examined the contribution of the three perisomatic interneuron types—the parvalbumin-containing fast-spiking basket cells (FSBCs) and axo-axonic cells (AACs), as well as the cholecystokinin-containing regular-spiking basket cells (RSBCs) to cholinergically induced oscillations in hippocampal slices, a rhythmic activity that captures several features of the gamma oscillations recorded *in vivo*. By analyzing the spiking activities of single neurons recorded in parallel with local field potentials, we found that all three cell types fired phase locked to the carbachol-induced oscillations, although with different frequencies and precision. During these oscillations, FSBCs fired the most with the highest accuracy compared with the discharge of AACs and RSBCs. In further experiments, we showed that activation of μ-opioid receptors by DAMGO ([D-Ala^2,N-Me-Phe^4,Gly^5-ol]enkephalin acetate), which significantly reduced the inhibitory, but not excitatory, transmission, suppressed or even blocked network oscillations both *in vitro* and *in vivo*, leading to the desynchronization of pyramidal cell firing. Using paired recordings, we demonstrated that carbachol application blocked GABA release from RSBCs and reduced it from FSBCs and AACs, whereas DAMGO further suppressed the GABA release only from FSBCs, but not from AACs. These results collectively suggest that the rhythmic perisomatic inhibition, generating oscillatory fluctuation in local field potentials after carbachol treatment of hippocampal slices, is the result of periodic GABA release from FSBCs.

Introduction

Cortical activities are organized and temporally segmented by several overlaid and embedded oscillations with different frequencies (Steriade, 2006). In awake brain, oscillations at gamma frequencies (30–100 Hz) recorded in different cortical areas have been found to emerge during sensory encoding, neuronal assembly formation, or memory storage and retrieval (Tiitinen et al., 1993; Sederberg et al., 2003; Montgomery and Buzsáki, 2007). The importance of gamma oscillations has been emphasized in cognitive processes such as feature binding (Singer, 1993) and in changes of synaptic weights, since they could provide a temporal frame for spike time-dependent plasticity (Paulsen and Moser, 1998). Although some insights into mechanisms of these rhythmic activities have been recently achieved (Hájos and Paulsen, 2009), the identity of inhibitory neuron types involved in the oscillogenesis is not yet established unequivocally.

One of the most studied *in vitro* models of gamma oscillations is the carbachol (CCh)-induced network oscillation in the CA3 area of the hippocampus, which is a brain region capable of intrinsically generating rhythmic activities *in vivo* and in slices (Fisahn et al., 1998; Csicsvari et al., 2003; Maier et al., 2003). It was proposed that gamma oscillations are the result of the precisely timed feedback interaction among pyramidal cells and GABAergic interneurons (Hájos et al., 2004; Mann et al., 2005; Oren et al., 2006). Current source density analysis combined with imaging of membrane potential fluctuation of pyramidal cells revealed that local field potentials (LFPs) are primarily generated by perisomatic inhibitory currents (Mann et al., 2005).

Perisomatic inhibitory interneurons (Freund and Katona, 2007; Klausberger and Somogyi, 2008) that synapse on the proximal dendrites and somata of principal neurons or on their axon initial segments are in strategic position to control action potential generation (Cobb et al., 1995; Miles et al., 1996). In cortical structures, three types of these GABAergic cells can be identified: the parvalbumin (PV)-containing fast-spiking basket cells

Received Aug. 6, 2010; accepted Sept. 1, 2010.

This work was supported by the Wellcome Trust, the Hungarian Scientific Research Fund (OTKA T049517, NNF78917, K 060927, K 81357), the National Office for Research and Technology (OMFB-01678/2009, NKTH-ANR Neurogen), the European Union (LSHM-CT-2004-005166), and the Howard Hughes Medical Institute. We are grateful to Prof. B.L. Kieffer for providing MOR KO mice for our study. We also thank Erzsébet Gregori, Emőke Szépné Simon, Zoltánné Lengyel, and Győző Goda, Richárd Fiáth, and Bálint P. Kerekes for their excellent technical assistance.

Correspondence should be addressed to Norbert Hájos, Laboratory of Network Neurophysiology, Institute of Experimental Medicine, Hungarian Academy of Sciences, Szigony u. 43, H-1083, Budapest, Hungary. E-mail: hajos@koki.hu.

DOI:10.1523/JNEUROSCI.4104-10.2010

 0270-6474/10/3015134-12$15.00/0

(FSBCs) and axo-axonic cells (AACs), as well as the cholecystokinin (CCK)-expressing regular-spiking basket cells (RSBCs) (Freund and Katona, 2007). Any of them could potentially contribute to oscillogenesis at gamma frequencies. Recent studies modifying the behavior of PV-containing inhibitory neurons using molecular biological techniques demonstrated the importance of these GABAergic cells in the generation of gamma oscillation (Fuchs et al., 2007; Cardin et al., 2009). However, neither approach could differentiate between the contribution of FSBCs and AACs, since both cell types express PV. In addition, the participation of CCK-expressing RSBCs in oscillogenesis has not been addressed either.

In this study, we aimed to clarify the involvement of these three types of interneurons in the generation of CCh-induced network oscillation (Oren et al., 2010). To reveal the firing properties of distinct neuron types during oscillation, we recorded local field potentials and spiking activity of identified inhibitory neurons from hippocampal slices. Using paired recordings from perisomatic inhibitory interneurons and pyramidal cells as well as pharmacological manipulations of oscillation, we found that FSBCs are responsible for most of the perisomatic inhibitory currents during the CCh-induced oscillations in the CA3 region of the hippocampus.

Materials and Methods

All experiments were performed in accordance with the Hungarian Act of Animal Care and Experimentation (1998, XXVIII, section 243/1998) and with the guidelines of the institutional ethical code.

Transgenic animals. Two transgenic mouse strains were used to selectively obtain recordings from perisomatic inhibitory cells. FSBCs and AACs were sampled in a strain where enhanced green fluorescent protein (EGFP) expression was controlled by PV promoter (Meyer et al., 2002), whereas RSBCs were recorded in another strain where EGFP was expressed under GAD65 promoter (López-Bendito et al., 2004). In addition, μ-opiate receptor (MOR) knock-out (KO) mice (Matthes et al., 1996) were used to test the specificity of DAMGO ([D-Ala^2,N-Me-Phe^4,Gly^5-ol]enkephalin acetate) effects, which were compared with the effects obtained in their wild-type (WT) littermates.

In vitro *electrophysiological experiments.* C57BL/6 and transgenic mice of both sexes (postnatal day 15–22) were deeply anesthetized with isoflurane and decapitated. Following decapitation, the brain was quickly removed into ice-cold cutting solution containing the following (in mM): sucrose, 252; KCl, 2.5; $NaHCO_3$, 26; $CaCl_2$, 1; $MgCl_2$, 5; NaH_2PO_4, 1.25; glucose, 10, bubbled with carbogen gas. Horizontal hippocampal slices were prepared using a Leica VT1000S or VT1200S microtome and placed into an interface-type holding chamber containing standard artificial CSF (ACSF) at 35°C that gradually cooled down to room temperature (~1–1.5 h). To induce oscillations with CCh, 300–350-μm-thick slices were cut. To characterize cellular interactions from identified cell pairs or other mechanisms of DAMGO actions, we cut 200–250-μm-thick slices to reduce the connectivity in the slice, since the high spontaneous activity evoked by CCh could have influenced the analysis of synaptic events.

The standard ACSF had the following composition (in mM): 126 NaCl, 2.5 KCl, 1.25 NaH_2PO_4, 2 $MgCl_2$, 2 $CaCl_2$, 26 $NaHCO_3$, and 10 glucose, prepared with ultra pure water and bubbled with 95% O_2/5% CO_2 (carbogen gas), pH 7.2–7.4. Recordings from cell pairs and the measurements of synaptic currents were made in submerged-type slice chambers (Luigs & Neumann), while oscillations were induced in a dual-superfusion chamber (Supertech) at room temperature with a flow rate of 2–4 ml/min (Hájos et al., 2009).

Oscillations were induced by bath application of 5 μM CCh. Patch pipettes (≈ 4–6 MΩ) filled with ACSF were used to monitor local field potentials and action potentials extracellularly. The field pipette was placed in stratum (str.) pyramidale of CA3. To record from identified interneuron subtypes, slices were cut from transgenic animals. EGFP-expressing neurons were identified using epifluorescence and differential interference contrast on an Olympus BX61 microscope. A second pipette was used to record spiking activity in a loose-patch configuration from the visually identified neurons. Action potentials were recorded for at least 60 s. The pipette was then withdrawn from the slice, and the same cell was patched with a new pipette filled with intrapipette solution containing the following (in mM): K-gluconate 138; CsCl 3; phosphocreatine 10; ATP 4; GTP 0.4; HEPES 10; QX-314 0.2; biocytin 3 mg/ml, adjusted to pH 7.3–7.35 using KOH (285–290 mOsm/L). Whole-cell series resistance was in the range of 5–15 MΩ. Both extracellular and whole-cell recordings were performed with a Multiclamp 700B amplifier (Molecular Devices), with the exception of experiments presented in supplemental Figure 7 (available at www.jneurosci.org as supplemental material), where field potentials were recorded with a BioAmp amplifier (Supertech). To detect EPSCs more reliably in pyramidal cells during oscillation, picrotoxin (600–650 μM) was included in the pipette solution (Nelson et al., 1994). Voltage measurements were not corrected for a junction potential. Both field and unit recordings were low-pass filtered at 2 kHz using the built-in Bessel filter of the amplifier. Data were digitized at 6 kHz with a PCI-6042E board (National Instruments) and recorded with EVAN 1.3 software (courtesy of Prof. I. Mody, University of California Los Angeles, Los Angeles, CA). All data were analyzed off-line using custom-made programs written in MATLAB 7.0.4 and Delphi 6.0.

Calculating peak-to-peak amplitude of the oscillation. To calculate the amplitude of the oscillation, an amplitude distribution histogram was made on a 60 s, 1 Hz, high-pass filtered section of the recording. The voltage range containing 95% of the points was used as peak-to-peak amplitude.

Firing-phase calculation. A custom-written firing phase detection algorithm was used. Spikes recorded in a loose-patch mode were detected by manually setting the threshold on the unfiltered trace. The negative peak of the trough of the oscillation was considered as phase zero. However, the position of the negative trough of an oscillation depends on how the original signal is filtered. In *in vivo* studies (Buzsáki et al., 2003) for gamma detection, the field potential is filtered with a relatively narrow (30–80 Hz) bandpass (BP) filter. Filtering at such a low frequency distorts the shape of the gamma oscillation and makes the original asymmetric wave shape symmetric, similar to a harmonic oscillation (supplemental Fig. 4*b*, available at www.jneurosci.org as supplemental material). We therefore detected the negative peak of the oscillation on field potentials digitally bandpass filtered between 5 and 500 Hz. We chose the negative peak of the oscillation as zero, because it has functional significance. Pyramidal cells start to fire in high synchrony in this phase (Hájos et al., 2004; Mann et al., 2005; Oren et al., 2006). Also at this point, the extracellular potential rises very quickly and defines phase zero very well. If the signal is low-pass filtered at gamma frequencies (as in the *in vivo* studies), this sharp negative peak will disappear and the position of the zero phase will be influenced by potential changes throughout the full cycle as well as by variable gamma cycle length (Atallah and Scanziani, 2009), all spoiling functionally meaningful zero phase definition.

The phase of individual spikes was specified by calculating the position of the unit spikes in relation to two subsequent negative phase times. Here again, care has to be taken, since the amplitude and the instantaneous frequency of the oscillation vary, and often the detection algorithm might skip one or more oscillation cycles. This would result in an erroneous shift in spiking phase toward zero.

Therefore, our spike phase detection algorithm checked for the actual detected cycle length and assigned a phase to a spike only if the actual cycle length did not differ from the mean of the average cycle length by more than a chosen fraction of the SD of the cycle length. Heuristically, we found that if we chose 0.3 SD, we achieved a feasible phase calculation. If there is no oscillation length checking, as a result of the skipped cycles, firing phase is shifted toward zero. If the detection algorithm is too strict (not allowing jitter), spikes during short or long oscillatory cycles are discarded (can be rather high portion), and the phase coupling will be very high but does not represent physiological values.

Since the oscillations in our experiments had a mean frequency of 15.2 ± 0.5 Hz ($n = 15$) at room temperature, to relate our results to *in vivo* data we mimicked the narrow BP filtering with a 5–30 Hz BP filter and also calculated the phase of the spikes this way. The cell groups

showed the same overlap in their phase, but the firing phase of the cell groups was shifted in the positive direction (due to the fact that low-pass filtering of the saw teeth-like oscillations shifted the negative peak to the negative direction).

In vivo *recordings.* Adult mice ($n = 4$) were used for the *in vivo* experiments. In each animal, injections of DAMGO and saline were made into the CA3 area of the hippocampus in approximate stereotactic anteroposterior and mediolateral coordinates: 3.0 and 3.0 mm, respectively. The dorsoventral position (usually 3.0 mm) was identified by the electrophysiological recordings, guided by the appearance of the large-amplitude gamma oscillations in LFP recordings. At the end of the experiments, the animals were killed and the brains removed; histology confirmed the localization of the electrodes.

Anesthesia was induced in isoflurane atmosphere followed by the intramuscular injection of a mixture of ketamine and xylazine (100 and 10 mg/kg, respectively), maintained by repeated (approximately every 30 min) intramuscular administration of the same substance. Body temperature was kept at 37°C with a heating pad. The head was held by a mouse adaptor affixed to a stereotaxic frame (David Kopf Instruments). Midline incision was made on the scalp exposing the skull, followed by retraction of the skin and craniotomy to expose a part of the left hemisphere. The dura was left intact, and room temperature saline solution was used to prevent desiccation.

Sixteen channel laminar multielectrodes equipped with two inner cannulae (40-μm-diameter glass capillaries) were used to record field potentials and to deliver DAMGO and saline solution. The injector electrode was lowered through the intact dura to target the CA3 region using a microdrive. Interelectrode spacing was 100 μm, electrode site diameter was 25 μm, shaft diameter was 350 μm, and the drug delivery site was located between contacts 10 and 11. The cannulae were attached to two calibrated micrometer driven 10 μl syringes (Hamilton Company) via a 250-μm-inner diameter Tygon tube (Saint-Gobain). Separate cannulae were carefully forward- and back-filled with DAMGO and saline to avoid air bubbles in the tubes.

LFP (0.03 Hz-5000 Hz) was recorded from each of the 16 contacts, sampled at a 20 kHz/channel rate with 16 bit precision (LabView, National Instruments) and stored on hard drive for off-line analysis. Current source density (CSD) analysis identifies synaptic/transmembrane generators of LFP, using high-resolution maps of simultaneously recorded field potentials obtained across a laminated neural structure. Inhomogeneous conductivity was not taken into account, second spatial derivative was calculated by the nearest neighbor method, and high-spatial frequency noise was reduced by Hamming-window smoothing (Ulbert et al., 2001). Artifact-free single sweep CSD epochs (1024 ms long) were averaged ($n > 300$) in the frequency domain to obtain the power spectrum. The spatial location of the largest CSD sinks in the gamma band was regarded as the indicator of the pyramidal layer. CSD power spectra before and after DAMGO (1 mM) and saline pressure injection (200–400 nl) were compared at this location using Student's paired t test, and significance level was set to $p = 0.001$ (Scan4.3 Edit, Compumedics).

Paired recordings. The intrapipette solution used for the presynaptic perisomatic inhibitory cells contained the following (in mM): potassium-gluconate 110, NaCl 4, Mg-ATP 2, HEPES 40, GTP 0.3, 0.2% biocytin, adjusted to pH 7.3 using KOH (290 mOsm/L). The intracellular solution used for the postsynaptic pyramidal cells contained the following (in mM): CsCl 80, Cs-gluconate 60, $MgCl_2$ 1, Mg-ATP 2, NaCl 3, HEPES 10, and QX-314 5, adjusted to pH 7.3 with CsOH (295 mOsm/L). Presynaptic interneurons were held in a current-clamp mode at ~ -65 mV and stimulated by brief current pulses (1.5 ms, 1–2 nA). Pyramidal cells were held in a voltage-clamp mode at a potential of -65 mV. Access resistance was frequently monitored and compensated between 65 and 75%, and cells that changed substantially >25% during recording were discarded from further analyses. In experiments with CCh, occasionally 5 μM NBQX (nitro-2,3-dioxo-benzo[f]quinoxaline-7-sulfonamide) was added to the bath solution to reduce the high background activity or to eliminate oscillations. The effect of CCh on inhibitory transmission was tested at 2 and 5 μM in the pairs of fast-spiking interneurons and pyramidal cells, whereas CCh was added only at 5 μM for the pairs of RSBCs and pyramidal cells. We found that CCh at 2 and 5 μM indistinguishably reduced the IPSC amplitude compared with the control values for both FSBCs and AACs (FSBC at 2 μM: 49.1 ± 6.9% of control, $n = 6$; at 5 μM: 42.3 ± 2.4% of control, $n = 8$, $p = 0.32$; AAC at 2 μM: 31.9 ± 3.2% of control, $n = 9$; at 5 μM: 36.5 ± 5.8% of control, $n = 8$, $p = 0.49$, t test); therefore, data within each group were pooled and compared with those data obtained in experiments of RSBC–pyramidal cell pairs.

Measurements of evoked and miniature events. In the presence of CCh, electrically evoked or miniature IPSCs were pharmacologically isolated by bath application of 3 mM kynurenic acid to block ionotropic glutamate receptors. To isolate evoked EPSCs and to prevent epileptiform discharges in CA3, $GABA_A$ receptor-mediated currents were blocked intracellularly by including picrotoxin (600–650 μM) in the pipette solution. We experienced that 10–15 min was enough after break-in to eliminate IPSCs. To measure miniature events, 0.5 μM tetrodotoxin (TTX) was included in the bath solution.

Drugs. All salts and drugs were obtained from Sigma-Aldrich, except TTX, CTAP (D-Phe-Cys-Tyr-D-Trp-Arg-Thr-Pen-Thr-NH2), and DAMGO, which were purchased from Tocris Bioscience. TTX, CTAP, and DAMGO were dissolved in water in 100 mM concentration and stored at −20°C.

Statistical analysis. Unless it is indicated, a Student's paired t test was used to compare the changes in IPSC amplitude, firing characteristics, cell membrane property parameters, and oscillation power after drug application. Data are presented as mean ± SEM. The Kolmogorov–Smirnov test was used to compare two cumulative distributions. Circular statistics were used to calculate cell firing phase and phase coupling. ANOVA was used to compare multiple datasets.

Anatomical identification of biocytin-filled neurons. After intracellular recording and biocytin filling, the slices was fixed in 4% paraformaldehyde in 0.1 M phosphate buffer (PB; pH 7.4) for at least 30 min, followed by washout with PB several times, and incubation in cryoprotecting solution (30% sucrose in 0.01 M PB) for 2 h. Slices were then freeze-thawed three times above liquid nitrogen and treated with 1% H_2O_2 in PB for 15 min to reduce endogenous peroxidase activity. For single stainings, filled cells were visualized using avidin-biotinylated horseradish peroxidase complex reaction (ABC; Vector Laboratories) with nickel intensified with 3-3-diaminobenzidine tetrahydrochloride (0.05% solution in Tris buffer, pH 7.4; Sigma) as a chromogen giving a dark reaction product. After dehydration and embedding in Durcupan (Fluka), neurons were identified based on their dendritic and axonal arborization, and some representative cells were reconstructed with the aid of a drawing tube using a 40× objective.

Fluorescent immunohistochemistry and electron microscopy. After recordings, the slices were fixed in a fixative containing 4% paraformaldehyde, in 0.1 M PB, pH 7.4, at 4°C. Before processing, the fixative was thoroughly washed out with 0.1 M PB. Slices were then cryoprotected in 30% sucrose, freeze-thawed over liquid nitrogen, embedded in agar, and resectioned at 60 μm thickness. Every third section was processed for electron microscopy: biocytin was visualized using the avidin–biotinylated–HRP complex (Vector Laboratories) and 3-3-diaminobenzidine tetrahydrochloride (0.05% solution in Tris buffer, pH 7.4) as a chromogen. Sections were then postfixed in 1% OsO_4, stained in 1% uranyl acetate, dehydrated in a graded series of ethanol, and embedded in epoxy resin (Durcupan; Sigma). Ultrathin sections of 60 nm thickness were cut for electron microscopy, and the postsynaptic target of 5–10 boutons of each recorded cell was identified. The remaining sections were processed for fluorescent double labeling (for details, see Lorincz and Nusser, 2008). They were treated with 0.2 mg/ml pepsin (catalog #S3002; Dako) in 0.2 M HCl at 37°C for 5 min and were washed in 0.1 M PB. Sections were blocked in normal goat serum (NGS) (10%) made up in Tris-buffered saline (TBS), pH 7.4, followed by incubations in mouse anti-ankyrin G (1:100, Santa Cruz Biotechnology) diluted in TBS containing 2% NGS and 0.3% Triton X-100. Following several washes in TBS, Cy3-conjugated goat anti-mouse (1:500; Jackson ImmunoResearch) was used to visualize the immunoreactions, and Alexa488-conjugated streptavidin (1:500; Invitrogen) to visualize the biocytin. Sections were then mounted on slides in Vectashield (Vector Laboratories). Images were taken using

an AxioImager.Z1 (Zeiss). All interneurons recorded in PV-EGFP mice were identified with this method.

Results

Identification of inhibitory neurons innervating the perisomatic area of CA3 pyramidal cells using EGFP-expressing transgenic mice and immunostaining for ankyrin G

To study the role of the three types of perisomatic inhibitory interneurons (Fig. 1) in the generation of CCh-induced oscillation, we used transgenic mice strains in which these neurons were selectively labeled with EGFP. PV-containing interneurons (FSBCs and AACs) were identified in slices from mice where EGFP expression was driven by PV promoter (Meyer et al., 2002), whereas RSBCs were targeted in slices from animals where GAD65 promoter regulated the expression of EGFP (López-Bendito et al., 2004). During recordings, all neurons were filled with biocytin and visualized *post hoc*. Only interneurons with axonal arbor restricted to the str. pyramidale and inner str. radiatum and oriens were included in this study (Fig. 1*a*). To unequivocally distinguish the FSBCs and AACs, we performed *post hoc* double-immunofluorescent labeling for biocytin and the scaffolding protein ankyrin G. This protein anchors different channels, including voltage-gated sodium channels (Nav1.2 and 1.6) in the axon initial segments (AISs) of neurons, allowing their selective visualization at light microscopic level (Jenkins and Bennett, 2001).

From a total number of 61 PV-EGFP cells recorded in different sets of experiments, in 30 cases the biocytin-filled boutons were localized to str. pyramidale and only rarely approached ankyrin G-stained profiles (Fig. 1c_{1-3}) suggesting their FSBC origin. Conversely, in the remaining 31 cases the axonal arbor was densest in str. pyramidale and neighboring str. oriens border, and the boutons formed close appositions with ankyrin G-immunoreactive segments, often in climbing-fiber manner, similar to the axon terminals of AAC (Fig. 1$d_{1,2}$). To identify the postsynaptic target of these cells, we performed electron microscopic examination on consecutive sections. In those cases where the immunofluorescent reaction showed only rare appositions, boutons mostly synapsed on pyramidal cell soma and proximal dendrites ($n = 5$) (Fig. 1c_4; supplemental Fig. 1, available at www.jneurosci.org as supplemental material), whereas in those cases where tight appositions were visible, boutons synapsed exclusively on AISs of the principal neurons ($n = 5$) (Fig. 1$d_{3,4}$; supplemental Fig. 1, available at www.jneurosci.org as supplemental material), which can be unequivocally identified upon having membrane undercoating and microtubule fascicles (Somogyi et al., 1983). As electron microscopic examination verified the double-immunofluorescent labeling as a powerful tool for the identification of FSBCs and AACs, the remaining 25 FSBCs and 26 AACs were identified only with this method.

Perisomatic inhibitory cell types have distinct firing characteristics during CCh-induced network oscillations

To induce oscillatory activity, a 5 μM CCh was bath applied and the local field potential was monitored extracellularly with an electrode placed in str. pyramidale. After a 10–15-min-long period, which was necessary for the full development of oscillations (Hájos et al., 2009), the local field potentials were recorded. To achieve necessary oxygenation of neurons, experiments were conducted at room temperature. Under these conditions, the peak-to-peak amplitude of the CCh-induced oscillations was 147.6 ± 7.12 μV with a power peak at 15.2 ± 0.5 Hz ($n = 15$). Although the frequency of CCh-induced oscillations at room temperature is in the beta frequency band (13–30 Hz), it falls into the gamma frequency range if recorded at higher temperature (see supplemental Figs. 2, 3, available at www.jneurosci.org as supplemental material) (Fisahn et al., 1998; Hájos et al., 2004). All other features of CCh-induced oscillations at room temperature and during temperature transitions resemble gamma oscillations recorded *in vitro* at 30−35°C or *in vivo* (Csicsvari et al., 2003; Mann et al., 2005; Hájos and Paulsen, 2009).

First, we examined the firing properties of the three types of perisomatic inhibitory interneurons in CA3 during cholinergically induced oscillatory activities. We recorded the spontaneous firing properties of EGFP-expressing neurons in a loose-patch mode (Fig. 2*a*,*b*). Using a whole-cell configuration, the same cell was then repatched and filled with biocytin for *post hoc* identification. Analysis of the results revealed that during oscillations the firing of the three cell types differed (Fig. 2*b–f*, Table 1). FSBCs fired single spikes almost at each oscillation cycle, in contrast to AACs and RSBCs, which often skipped cycles (Fig. 2*b*,*c*). On average, FSBCs discharged two action potentials (i.e., doublets) in every 10th cycle and AACs only occasionally fired doublets, while RSBCs very rarely did so (Fig. 2*d*). The phase of the action potentials (zero set to the negative peak of the oscillation recorded in str. pyramidale) of different cell types did not prove to be a distinguishing feature, since cells fired on the ascending phase of oscillations with their preferred phase varying within overlapping ranges (Fig. 2*e*; see also supplemental Fig. 4*a*, available at www.jneurosci.org as supplemental material). In contrast, there was a difference in the phase-coupling strength of the three cell types (Fig. 2*f*). FSBCs fired with high accuracy around the phase characteristic for the individual cells. The firing of AACs was less coupled to the oscillation, and RSBCs proved to be significantly less accurate in their firing than the other two cell types.

In summary, during CCh-induced synchronous activities in hippocampal slices, FSBCs were the most active perisomatic inhibitory cells and often fired doublets in a cycle, and their action potentials were the most strongly coupled to the oscillation.

DAMGO reduces CCh-induced network oscillations via μ-opioid receptors

Previous data showed that morphine could disrupt long-range synchrony of gamma oscillations in hippocampal slices via MORs (Whittington et al., 1998). Since these types of opioid receptors are selectively expressed on PV-immunopositive axon terminals (Drake and Milner, 2002) and their activation effectively reduced GABA release from fast-spiking interneurons with a much smaller effect on the inhibitory transmission of RSBCs (Glickfeld et al., 2008), activation of MORs could be a useful tool to separate the contribution of RSBCs from that of PV-containing perisomatic inhibitory cells in oscillogenesis.

First, we tested whether the activation of MORs could interfere with gamma oscillation recorded *in vivo*. To this end, we monitored local field potentials in anesthetized mice using a 16 channel laminar multielectrode equipped with two inner cannulae for solution applications. After obtaining the control period, 200–400 nl of saline or DAMGO (1 mM) was applied. Following DAMGO application, occasional interictal-like activity appeared with variable delays (10–60 s) in the recordings. Analyzing sections free of interictal episodes, we found that DAMGO significantly ($p < 0.001$) reduced the CSD gamma band power in the pyramidal cell layer, while saline did not induce significant changes (Fig. 3). These results indicate that DAMGO can effec-

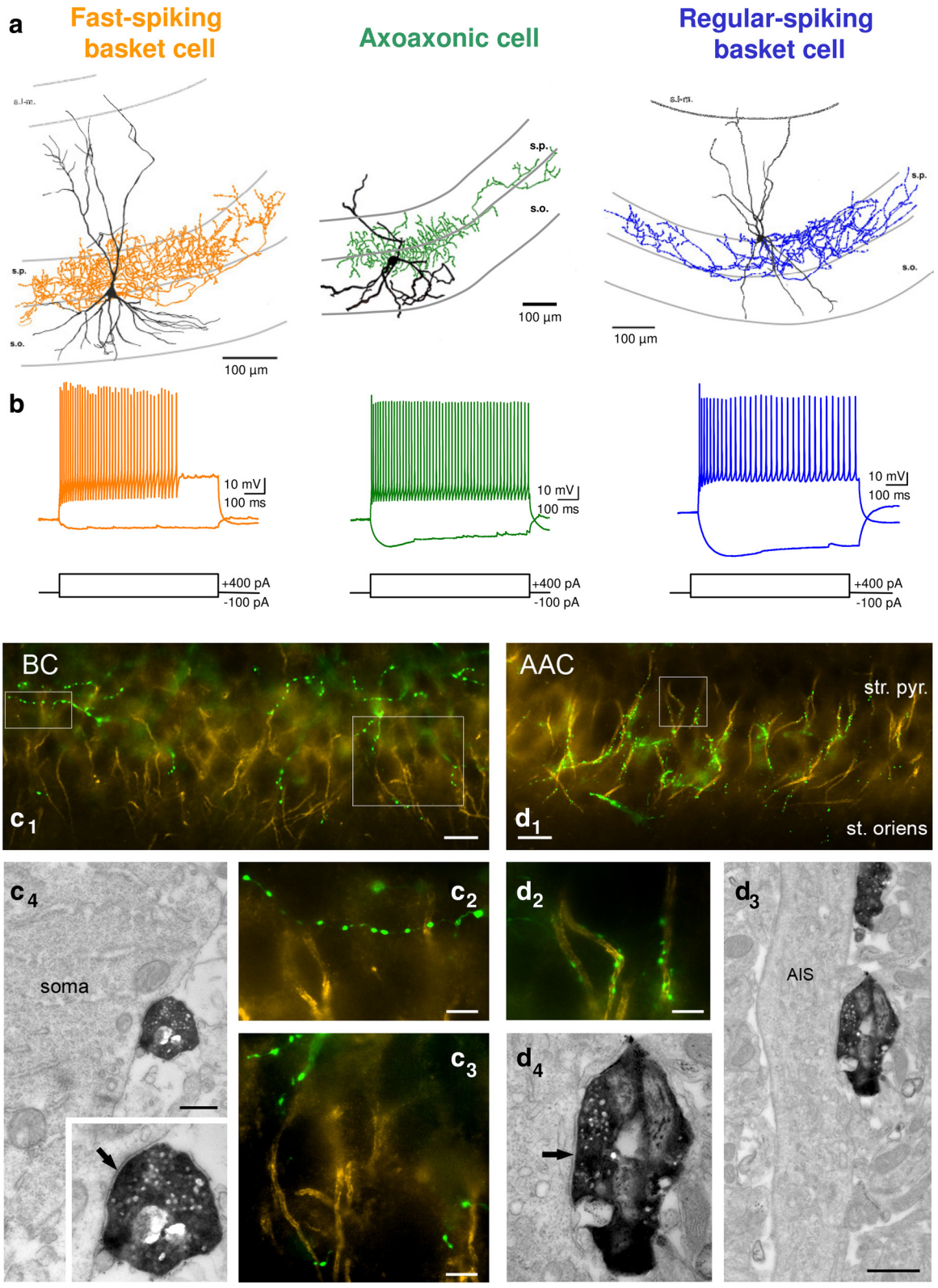

Figure 1. Three subsets of inhibitory neurons innervate the perisomatic region of CA3 pyramidal cells. ***a***, PV-containing FSBCs (orange) and AACs (green) as well as CCK containing RSBCs (blue). ***b***, The axonal (in color) and dendritic (in black) arbors of the three cell types are shown together with their response to depolarizing and hyperpolarizing current steps. Though the axonal arbor of the AACs is shifted toward str. oriens compared with the axonal arbor of basket cells, it is difficult to reliably separate the two cell types. ***c***, ***d***, Using double-fluorescent staining against ankyrin G (selectively labeling AISs) and biocytin (visualizing the axons of the filled cells), the difference between the two cell types can be resolved. While there is no, or very little, association between boutons of basket cells (c_{1-3}, green) and the ankyrin G-stained AISs of the pyramidal cells (yellow), bouton rows of the AACs ($d_{1,2}$, green) outline the axon initial segments of pyramidal cells. The target selectivity of the two cell types had been confirmed in serially sectioned electron microscopy slices (for 5 cells of both types). Axon terminals of FSBCs (c_4) contacted somata of pyramidal cells (arrow on inset shows synaptic specialization in higher magnification), while axon endings of AACs (d_3) innervated the axon initial segments of the same cell type and formed symmetrical synapses (d_4, arrow). Scale bars: c_1, d_1, 20 μm; $c_{2,3}$, d_2, 5 μm; c_4, d_3, 0.5 μm. s.l-m., str. lacunosum-moleculare; s.p., str. pyramidale; s.o., str. oriens.

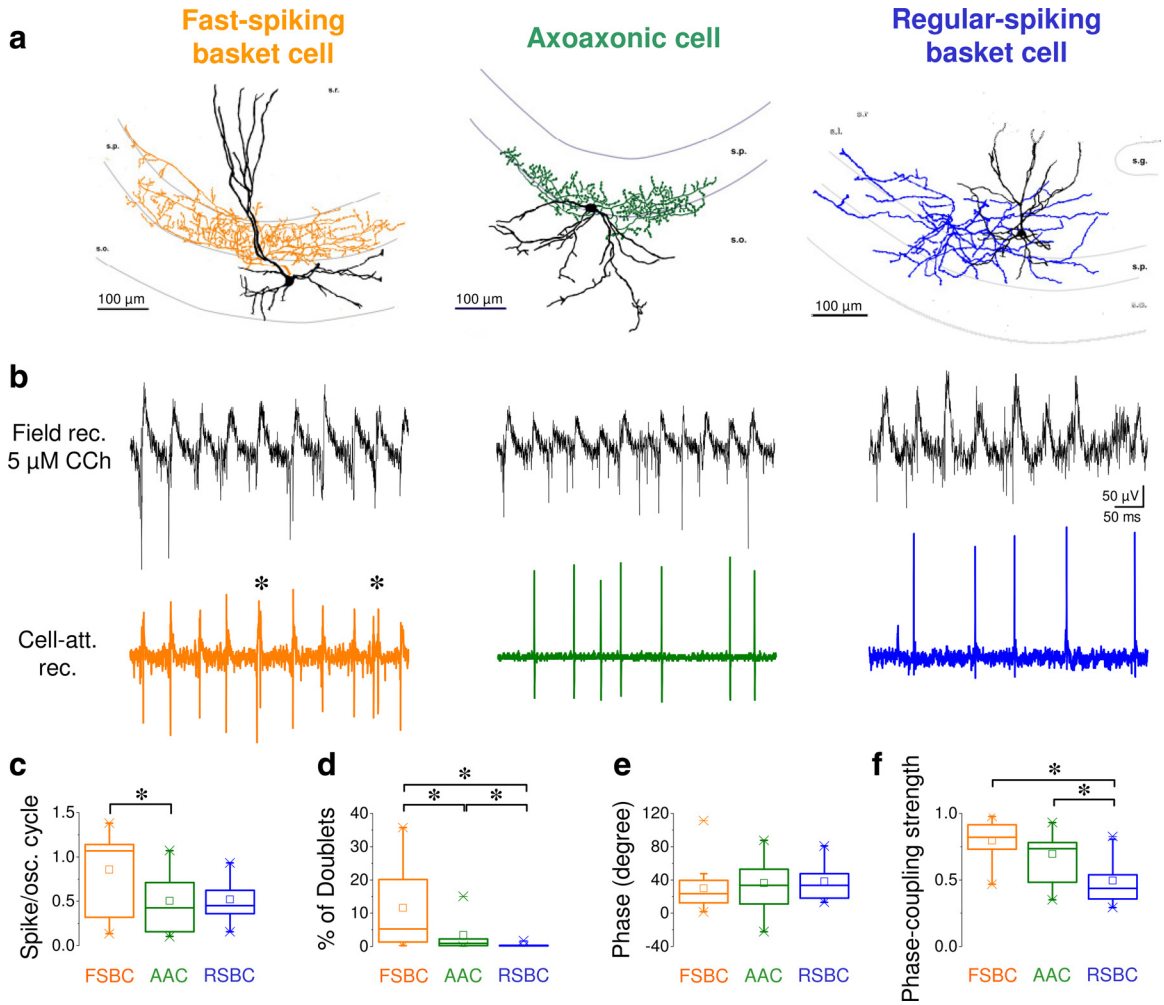

Figure 2. Subtypes of perisomatic inhibitory cells can be separated on the basis of their firing frequency, doublet incidence, and phase-coupling strength during CCh-induced network oscillations *in vitro*. ***a–c***, Concomitant recording of field oscillations and spikes in a loose-patch mode from different perisomatic inhibitory cells (***a***) showed that they fire phase locked to oscillations induced by CCh (***b***, ***c***). FSBCs (orange) often fired doublets (asterisks). ***c***, ***d***, The spikes per cycle (***c***) and the doublet ratio (***d***) were significantly higher for FSBCs ($n = 13$) than for AACs ($n = 12$, green) and RSBCs ($n = 10$, blue). Thus, FSBCs fired approximately once in every oscillation cycle. ***e***, ***f***, While the average phase of the individual cells varied around the ascending phase of the cycles (***f***) (see also supplemental Fig. 4*a*, available at www.jneurosci.org as supplemental material), and cell types could not be separated on the basis of their firing phase (***e***), the phase coupling (***f***) of FSBCs and AACs was significantly ($p = 0.001$ and 0.023, respectively) higher than that of the RSBCs. Polar plots showing the firing accuracy and phase of each recorded neurons are shown in supplemental Figure 4*a* (available at www.jneurosci.org as supplemental material). Here in ***c–f***, and also in Figures 7 and 8, the mean (small open square), the median (midline of the big box), the interquartile range (large box), the 5/95% values (ends of bars), as well as the minimal/maximal values (bottom and top X symbols) are shown on the charts. s.r., str. radiatum; s.l., str. lucidum; s.p., str. pyramidale; s.o., str. oriens; s.g., str. granulosum.

Table 1. Firing properties of the three types of perisomatic inhibitory cells during CCh-induced network oscillation

	FSBC ($n = 13$)	AAC ($n = 12$)	RSBC ($n = 10$)
Firing frequency (Hz)	15.01 ± 2.3	7.9 ± 1.3	9.42 ± 1.2
Spike/oscillation cycle	0.86 ± 0.13	0.51 ± 0.09	0.52 ± 0.08
Doublets (%)	11.6 ± 3.6	3.4 ± 1.4	0.4 ± 0.1
Phase (°)	29.9 ± 7.8	36.3 ± 8.4	38.1 ± 6.5
Phase-coupling strength	0.8 ± 0.04	0.69 ± 0.06	0.49 ± 0.06

Data are presented as mean ± SEM.

tively reduce gamma oscillations in the CA3 region of the intact hippocampus.

Next, we aimed to clarify how the MOR activation by DAMGO leads to the suppression of gamma oscillations. Therefore, we induced network oscillations by bath application of 5 μM CCh in hippocampal slices. To reproduce our *in vivo* findings, 1 μM DAMGO was added to the superfusate. This treatment effectively reduced the power or even fully eliminated the CCh-induced oscillations within 2–8 min both at room temperature (Fig. 4, left) and at 32−34°C (supplemental Fig. 5, available at www.jneurosci.org as supplemental material). To test the specificity of DAMGO action, CTAP, a MOR antagonist, was applied (200 nM) for 5 min preceding DAMGO. CTAP alone did not change the parameters of the oscillation, suggesting the lack of tonic MOR activation in our slice preparations, but prevented the effect of subsequently applied DAMGO (supplemental Fig. 6, available at www.jneurosci.org as supplemental material). If CTAP was applied after DAMGO-induced drop in oscillation power, it could fully reverse the effect of DAMGO in 5–10 min (supplemental Fig. 6, available at www.jneurosci.org as supplemental material). To further confirm that DAMGO acted exclusively via MORs, we repeated the experiments in MOR knock-out mice. We found no difference in the peak power (WT: 164.9 ± 26.3 μV^2/Hz, $n = 44$; KO: 161.17 ± 38.2 μV^2/Hz, $n = 19$; Mann–Whitney test, $p = 0.98$) or in the frequency of network oscillations (WT: 15.1 ± 0.7 Hz, $n = 44$; KO: 16.5 ± 0.8

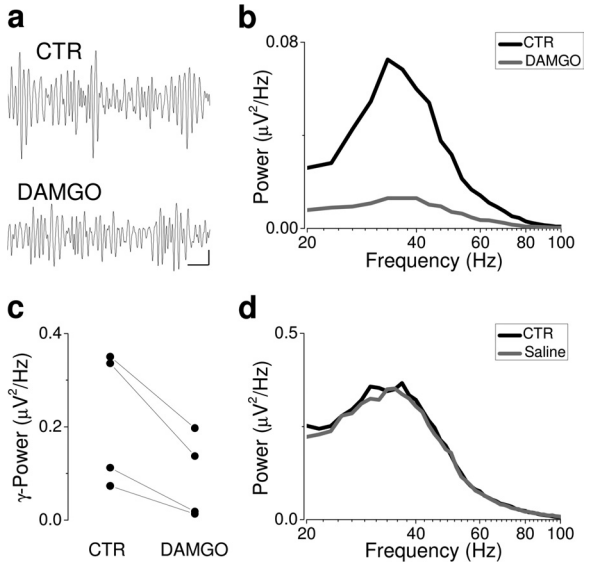

Figure 3. MOR activation suppresses gamma oscillations *in vivo*. ***a***, ***b***, Bandpass-filtered (between 35 and 45 Hz) *in vivo* recordings from the CA3 region of the hippocampus (***a***) and the corresponding power spectra before and after DAMGO application (***b***). The mean frequency of oscillations was 41.5 ± 2.9 Hz ($n = 4$). Calibration: 10 μV and 100 ms. ***c***, DAMGO significantly reduced the CSD gamma band power monitored in str. pyramidale [control (CTR), 0.217 ± 0.073 μV^2/Hz; DAMGO, 0.091 ± 0.045 μV^2/Hz; $n = 4$, $p < 0.001$]. ***d***, In contrast, saline application caused no significant change (CTR, 0.235 ± 0.115 μV^2/Hz; DAMGO, 0.231 ± 0.121 μV^2/Hz; $n = 2$).

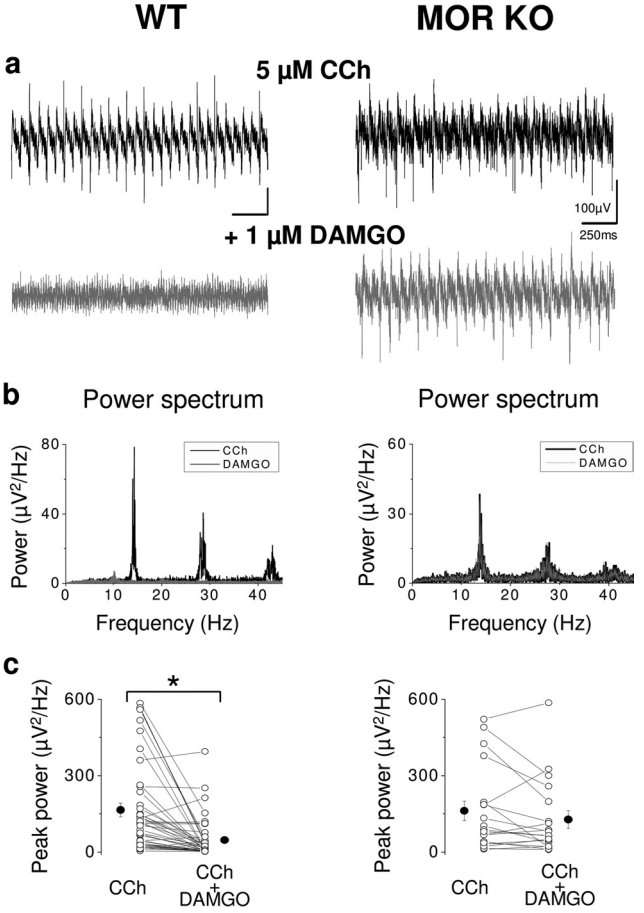

Figure 4. MOR activation blocks CCh-induced network oscillations *in vitro*. ***a***, CCh-induced oscillations (top row) were blocked by bath application of 1 μM DAMGO in the WT mouse (left), but not in MOR KO animals (right), indicating the specific action of DAMGO on MORs. ***b***, Power spectral density plots from the same experiment show a decrease in the power following DAMGO application in WT (left), but not in KO (right) animals. ***c***, Statistical analyses demonstrated a significant drop in the peak power in the WT (left, 164.9 ± 26.7 vs 46.7 ± 11.6 μV^2/Hz; $n = 44$; Wilcoxon signed rank test, $p < 0.0001$) but not in the KO animals (right, 161.7 ± 38.2 vs 127.3 ± 34.4 μV^2/Hz; $n = 19$; Wilcoxon signed rank test, $p = 0.15$).

Hz, $n = 19$; Mann–Whitney test, $p = 0.12$) between the KO and WT animals. In mice lacking MORs, DAMGO application had no detectable effect on the power and the frequency of the oscillations (Fig. 4, right). Thus, these data showed that DAMGO could effectively suppress CCh-induced oscillation, an effect that was mediated solely via MORs.

DAMGO application suppresses synaptic inhibition, which desynchronizes, but does not decrease, pyramidal cell activity

Field oscillations can break down either because the activity of neurons decreases, and thus currents responsible for the generation of the rhythmic field potentials disappear, or the firing of neurons desynchronizes and the currents do not sum up to give a detectable field signal. To get a deeper insight into the mechanisms of how DAMGO blocks oscillations and to distinguish these two possibilities, first we recorded local field potentials in str. pyramidale and simultaneously monitored multiunit activity that reflects mostly pyramidal cell firing (Fig. 5). While the peak power of oscillations was significantly reduced by DAMGO application (CCh: 86.4 ± 17.8 μV^2/Hz; CCh plus DAMGO: 18.6 ± 5.4 Hz; $n = 5$, $p = 0.006$), the frequency of multiunit firing did not change (CCh: 26.2 ± 9.3 Hz; CCh plus DAMGO: 24.2 ± 9.1 Hz; $n = 5$, $p = 0.54$), but, remarkably, unit synchrony disappeared, as shown by the multiunit autocorrelograms (Fig. 5). Though we could not identify the neurons participating in the multiunit spike assembly, they fired earlier in the oscillation phase (phase: 2.96 ± 1.13°; phase-coupling strength: 0.67 ± 0.054; $n = 5$) than the interneurons (Table 1), indicating that they were pyramidal cells (Hájos et al., 2004).

In the next set of experiments, we monitored local field potentials in str. pyramidale as well as EPSCs and IPSCs from two pyramidal cells (supplemental Fig. 7, available at www.jneurosci.org as supplemental material). The originally synchronized, phase-locked, large-amplitude, compound IPSCs decreased, or, as in the experiment shown in supplemental Figure 7 (available at www.jneurosci.org as supplemental material), largely fell below the detection threshold by DAMGO application (supplemental Fig. 7, bottom, available at www.jneurosci.org as supplemental material). Since the currents generating CCh-induced oscillations in the hippocampus predominantly originate from perisomatic inhibitory synapses (Mann et al., 2005; Oren et al., 2010), parallel to the IPSC amplitude decrease, the power of the oscillations also dropped, or completely disappeared (supplemental Fig. 7, top, available at www.jneurosci.org as supplemental material). During this transition, there was a much smaller change in the amplitude or in the frequency of EPSCs (or in the charge per cycle). However, the synchrony of the excitatory events decreased and disappeared, as shown on autocorrelograms (supplemental Fig. 7, middle, available at www.jneurosci.org as supplemental material).

These results together suggest that after the suppression of CCh-induced oscillations caused by DAMGO, pyramidal cell activity is mostly maintained, but their spikes are no longer phase locked to the oscillations due to the disappearance of periodic inhibitory control. Thus, the reduction of synaptic inhibition by DAMGO could decrease or abolish CCh-induced network oscillations.

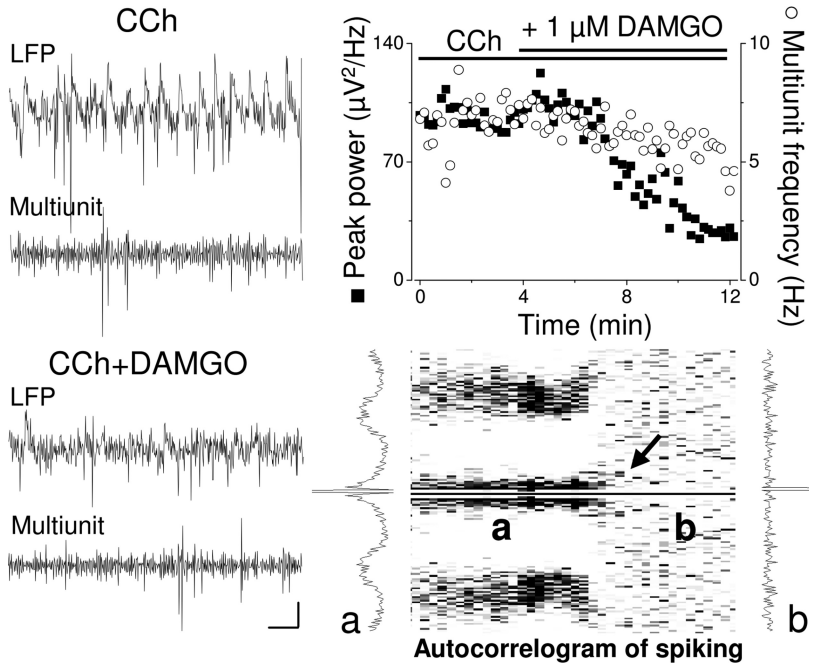

Figure 5. DAMGO application suppresses network oscillations: desynchronization of multiunit activity without changing firing frequency. The left column shows parallel recordings of field oscillations (top trace) and concomitant multiunit activity (filtered between 100 Hz and 2 kHz) during CCh-induced oscillation before and after DAMGO application. Calibration: 50 μV and 0.1 s. The time course of the same experiment is shown in the right column. While the wash-in of DAMGO caused a fast drop in the peak power of the oscillation, the frequency of multiunit activity only slightly decreased (top), but their synchronization was abolished (arrow) as indicated by the autocorrelograms (bottom).

DAMGO exerts its effect by reducing inhibitory transmission, but leaves excitatory transmission and pyramidal cell properties intact

The finding that DAMGO reduces synaptic inhibition is in agreement with earlier results (Masukawa and Prince, 1982; Cohen et al., 1992). However, to clarify the mechanisms underlying the effect of MOR activation on oscillation, we aimed to determine whether DAMGO exerts additional effects on the elements of CA3 neuronal network. First, we tested the effects of DAMGO on the basic properties of CA3 pyramidal cells. These neurons showed no significant change in their input resistance (in CCh: 370.0 ± 25.5 MOhm; in CCh plus DAMGO: 355.5 ± 9.83 MOhm; $n = 5$; $p = 0.53$) or in their membrane time constant (in CCh: 88.6 ± 8.58 ms; in CCh plus DAMGO: 90.5 ± 16.0 ms; $n = 5$; $p = 0.89$). We then examined the effects of DAMGO on evoked and miniature postsynaptic currents. As shown in Figure 6, in CA3 pyramidal cells DAMGO application caused a significant reduction in the amplitude of IPSCs evoked by electrical stimulation of fibers in str. pyramidale or at the border of str. pyramidale and lucidum. In contrast, MOR activation had no effect on EPSC amplitude evoked with the stimulation of fibers in str. radiatum. Similarly, in CA3 pyramidal cells a decrease was detected in the frequency of miniature IPSCs following DAMGO application, without a change in their amplitude distribution. No change could be detected in the frequency or amplitude of miniature EPSCs. For more details, see supplemental Figure 8 (available at www.jneurosci.org as supplemental material). Last, we examined whether the excitatory input on interneurons expressing PV could be affected by DAMGO. Similarly to the results obtained in CA3 pyramidal cells, the activation of MORs had no effect on the amplitude of evoked EPSCs recorded in three fast-spiking basket cells and two axo-axonic cells (in CCh: 202.7 ± 59.1 pA; in CCh plus DAMGO: 214.8 ± 73.3; $n = 5$, p = 0.72).

These results collectively demonstrated that DAMGO suppresses only inhibitory transmission, without affecting the excitatory synaptic communication and pyramidal cell excitability in the presence of CCh.

Cholinergic receptor activation differentially decreases transmitter release from perisomatic inhibitory cells

Our pharmacological experiments strengthened the hypothesis that PV-immunopositive perisomatic inhibitory cells expressing MORs could have a role in oscillogenesis. However, DAMGO caused a small but significant reduction in the IPSC amplitude recorded in RSBC–pyramidal cell pairs (Glickfeld et al., 2008); thus, the contribution of IPSCs to the perisomatic inhibitory currents generating CCh-induced network oscillations cannot be completely ruled out. Since all three types of perisomatic inhibitory interneurons fired at a similar phase of the oscillation cycles (though with different frequency and precision; Table 1), each cell group, in principle, could indeed contribute to the inhibitory currents, if GABA was released from their axon terminals under the conditions of CCh-induced oscillation. To address the question of the extent to which IPSCs originating from the three interneuron types might contribute to active current sources in the pyramidal cell layer (Mann et al., 2005), we examined their release properties in the presence of 5 μM CCh used to induce oscillations in this study.

We performed paired whole-cell recordings from presynaptic interneurons and postsynaptic pyramidal cells in the CA3 region (Fig. 7*a*). Regardless of the cell type, CCh application decreased the amplitude of postsynaptic currents. In the absence of CCh, the IPSCs of FSBCs and AACs showed short-term depression; the IPSCs of RSBCs did not. To approximate the conditions to continuous firing during ongoing oscillation, we compared the amplitude of the last five IPSCs, when the synaptic depression in FSBC– and AAC–pyramidal cell pairs reached steady-state levels (Fig. 7*b*). Statistical analysis revealed that CCh significantly ($p < 0.001$) suppressed the amplitude of the last five IPSCs in a cell-type-specific manner (Fig. 7*c*). Almost full reduction of IPSC amplitude was observed in RSBC–pyramidal cell pairs, whereas CCh exerted a smaller inhibition on the amplitude of IPSCs of AACs and FSBCs. The degree of reduction was significantly different among cell types ($p < 0.001$).

In line with earlier data (Fukudome et al., 2004; Neu et al., 2007), depression at synapses between RSBCs and pyramidal cells by CCh was the result of the activation of CB_1 cannabinoid receptors (CB_1R), since bath application of a CB_1R antagonist AM251 (1 μM) reversed the silencing effect of cholinergic receptor activation on IPSC amplitude (in CCh: 23.6 ± 16.1% of control; in CCh plus AM251: 89. 4 ± 19.5% of control; $n = 4$, $p = 0.04$).

These results suggest that, while RSBCs do fire during CCh-induced network oscillation, the GABA release from their axon terminals is almost completely muted as a result of CB_1R activation. Thus, the IPSCs originating from RSBCs can only minimally contribute to active current sources; therefore,

these perisomatic inhibitory cells do not play an active role in the generation of synchronous activities induced by cholinergic receptor activation.

DAMGO differentially affects GABA release from FSBCs and AACs in the presence of CCh

Immunocytochemical results showed that MORs are expressed in PV-immunopositive axon terminals synapsing on the somata or on the proximal dendrites of hippocampal pyramidal cells, but in the axon endings contacting axon initial segments the presence of MORs is questionable, as stated by Drake and Milner (2002). Since RSBCs do not participate in perisomatic current generation here, these data propose that the effect of DAMGO on oscillation could be due to the reduction of GABA release predominantly, if not exclusively, from the axon terminals of FSBCs.

To separate the possible contributions of FSBCs and AACs to oscillation generation, we subsequently applied DAMGO (together with CCh) after CCh treatment in paired recordings (Fig. 7). The amplitude of the last five IPSC in FSBC–pyramidal cell pairs were significantly depressed compared with the amplitude in the presence of CCh, but there was no further reduction in IPSC amplitudes observed in AAC–pyramidal pairs (Fig. 8*a*,*b*). Interestingly, the IPSC amplitude of FSBCs in the mixture of CCh and DAMGO was not significantly different from the IPSC amplitude of AACs in the presence of CCh or in CCh plus DAMGO ($p = 0.15$) (Fig. 8*c*).

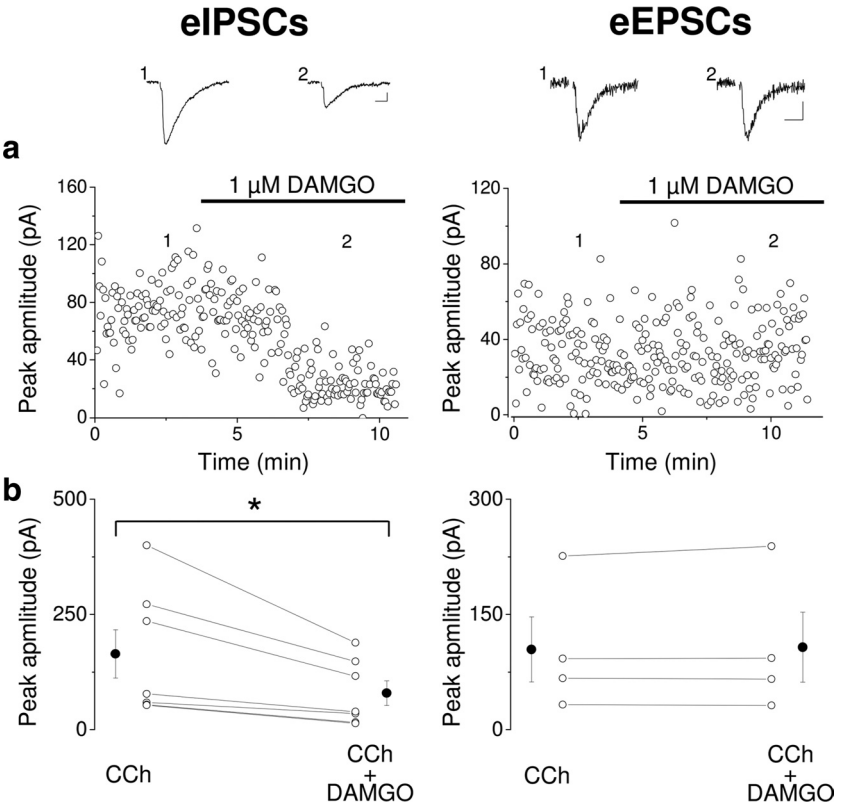

Figure 6. DAMGO reduces the amplitude of inhibitory, but not excitatory synaptic currents evoked by electrical stimulation in CA3 pyramidal cells. ***a***, Two examples showing that the bath application of DAMGO reduced the peak amplitude of evoked inhibitory synaptic currents (eIPSCs), leaving unaffected the amplitude of evoked excitatory synaptic currents (eEPSCs). Recordings were done in the presence of 5 μM CCh. Example traces are averaged records of six to eight consecutive events taken at the labeled time points. The stimulus artifacts were removed from the traces. Calibration: 10 pA and 10 ms. ***b***, In all tested cases, DAMGO application significantly reduced the amplitude of evoked IPSCs (left, 164.3 ± 52.38 vs 79.3 ± 26.68 pA in DAMGO, $n = 7$, $p = 0.017$) recorded from CA3 pyramidal cells elicited by electrical stimulation in str. pyramidale or at the border of str. radiatum and lucidum. In contrast, EPSCs elicited by electrical stimulation in str. radiatum showed no change following DAMGO application (right, 104.4 ± 42.3 vs 107.2 ± 45.6 pA in DAMGO, $n = 4$, $p = 0.45$).

These data demonstrate that in the presence of CCh DAMGO selectively suppressed GABA release from axon terminals of FSBCs, but not of AACs, and thus synaptic output of FSBCs is the major source of the perisomatic inhibitory currents, which generates CCh-induced field oscillation.

Discussion

In the present study, we provided several lines of evidence converging to the conclusion that FSBCs, but not RSBCs or AACs, play a central role in the generation of rhythmic field activities induced by CCh in hippocampal slices, as follows: (1) during CCh-induced network oscillations FSBCs fired the most with the highest accuracy compared with the discharge of AACs and RSBCs; (2) at the CCh concentration used to induce network oscillations, IPSCs of RSBCs were nearly completely eliminated, while IPSCs exerted by FSBCs and AACs were also reduced to a different extent; and (3) the MOR agonist DAMGO, which effectively blocked oscillations *in vitro* and *in vivo*, selectively reduced inhibitory currents of FSBCs, but not of AACs, in the presence of CCh.

The three types of perisomatic inhibitory interneurons fire within the same time window, but with different phase-coupling precision, during CCh-induced network oscillation

The analysis of the firing phases of cells (Fig. 2) showed that there is a considerable variation in the preferred firing phase of individual neurons within each type, and thus activity of the populations overlap. Most of the cells fire 0–60° after the negative peak of the oscillations (i.e., in the ascending phase, measured in str. pyramidale), following the discharge of pyramidal cells, consistent with the synaptic feedback model of pharmacologically induced oscillations in CA3 either in hippocampal slices (Hájos et al., 2004; Gloveli et al., 2005; Mann et al., 2005; Hájos and Paulsen, 2009) or in *in vivo* gamma (Csicsvari et al., 2003; Atallah and Scanziani, 2009). Based on population averages, FSBCs fired somewhat earlier, but the differences did not reach significance level. While the phase of firing did not differ among the three cell groups, their phase locking was distinct. FSBCs showed the strongest phase locking (0.8 ± 0.04), and RSBCs the weakest (0.49 ± 0.06). These differences found in the spiking accuracy of the two basket cell types match earlier findings. PV-containing basket cells (FSBCs) have a narrow input integration window, a precise input–output relationship, and synchronized transmitter release, in contrast to CCK-immunopositive basket cells (RSBCs), which have a wider input integration window and less accurate firing, and show asynchronous, delayed GABA release (Hefft and Jonas, 2005; Glickfeld and Scanziani, 2006; Daw et al., 2009). Regardless of whether the cells fire with high accuracy or not, since the preferred phase of individual cells within each population overlap, and a large number of perisomatic inhibitory cells converge onto a single pyramidal cell, principal neurons receive

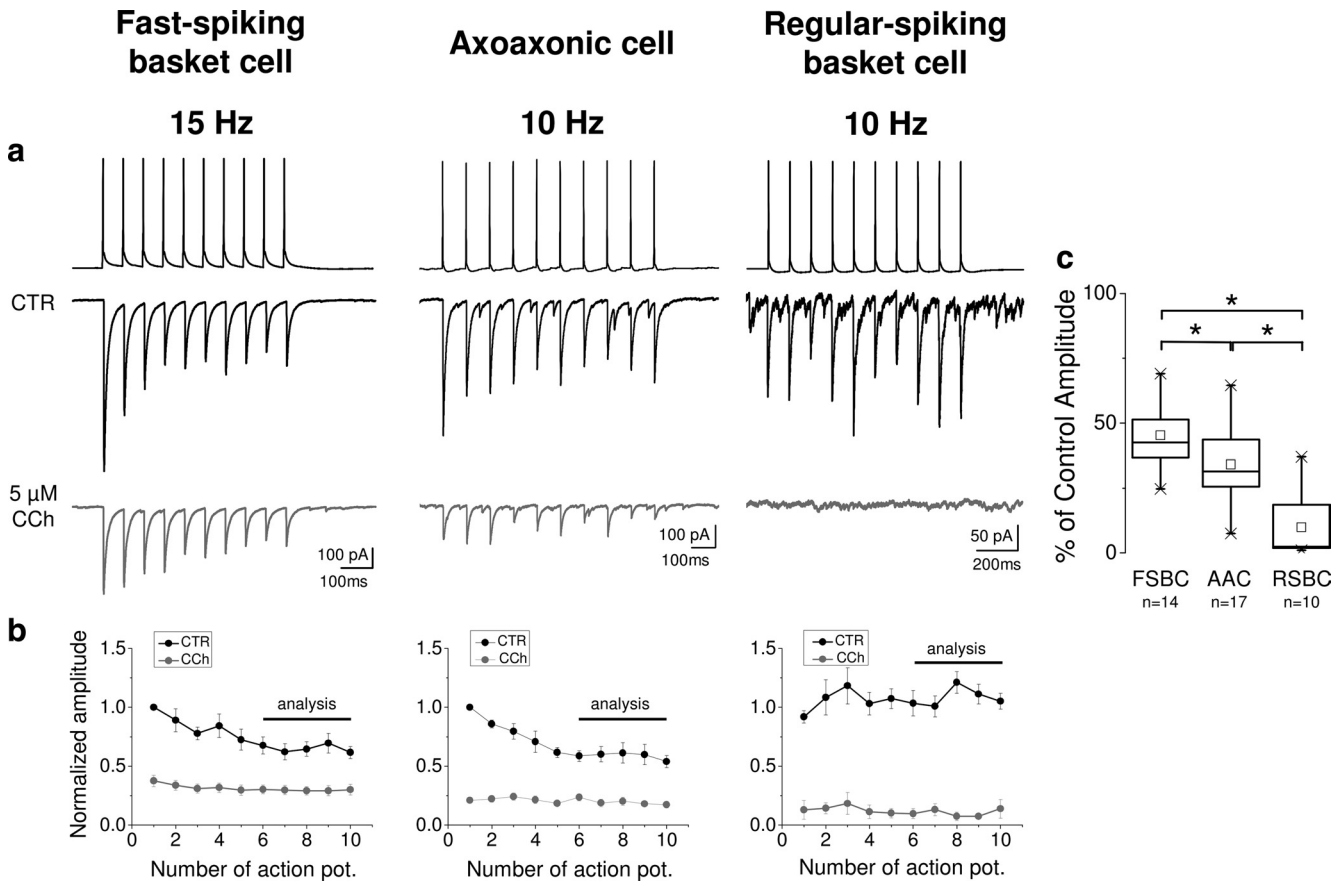

Figure 7. Cholinergic activation eliminates IPSCs originating from RSBCs and decreases synaptic inhibition mediated by FSBCs and AACs. Perisomatic inhibitory interneuron–pyramidal cell pairs had been recorded to test the effective inhibition exerted by different cell types on pyramidal cells, in conditions characteristic of CCh-induced network oscillation. Trains of 10 action potentials were evoked in each interneuron at different frequencies to record unitary IPSCs in their postsynaptic pyramidal cells first under control conditions (CTR), followed by bath application of CCh. After *post hoc* analysis of the cell's identity, the properties of IPSCs at the characteristic frequencies at which the given cell type would have fired during CCh-induced oscillations were analyzed (Table 1; action potentials evoked at 15 Hz for FSBCs, and at 10 Hz for AACs and RSBCs). ***a***, Action potentials evoked in identified cells shown in Figure 1 at frequencies characteristic of their firing during oscillatory activities elicited IPSCs in their postsynaptic pyramidal cell. ***a***, ***c***, Application of CCh reduced or eliminated IPSCs depending on the type of presynaptic inhibitory neurons. The GABA release from PV-containing neurons was depressing, which was decreased by CCh. RSBC synapses were facilitating/depressing, showing on average no short-term plasticity, and their release was almost completely blocked by CCh application. ***b***, To analyze the effect of CCh on steady-state release, the 6th to 10th evoked IPSCs were averaged and compared. ***c***, All reductions were significant (ANOVA, $p = 0.001$) and differed from each other. IPSCs evoked by the RSBCs were almost completely eliminated (9.9 ± 3.8% of control, $n = 10$, $p = 0.001$). In the case of PV-containing cells, where transmission persisted, there was a stronger reduction for AACs (34.1 ± 3.1% of control, $n = 17$, $p = 0.001$) than for FSBCs (45.2 ± 3.3% of control, $n = 14$, $p = 0.001$).

inhibitory currents during the first half of the gamma cycle both *in vitro* and *in vivo* (Atallah and Scanziani, 2009; Hájos and Paulsen, 2009).

We found that the phase coupling of the three types of perisomatic inhibitory interneurons in CA3 was considerably higher (0.80–0.49) than measured in the CA1 area *in vivo* during gamma oscillations (0.23–0.07) (Tukker et al., 2007; Klausberger and Somogyi, 2008). Still, the relative modulation depth of firing of these cell types is similar *in vivo* and *in vitro*, since FSBC had the highest modulation, while RSBCs the lowest.

Several explanations can be proposed for the difference in the modulation depths, as follows: (1) *in vitro*, the strength of gamma modulation of interneuronal firing in the CA1 area is weaker than in the CA3 area (R. Zemankovics, J. Veres, I. Oren, and N. Hájos, unpublished observations), most probably because gamma activity is generated in CA3 and only spreads into CA1 (Csicsvari et al., 2003); (2) differences in the recording and signal-processing methods used in *in vivo* and in this study; (3) *in vivo*, there are several network activity patterns embedded in each other that might result in weaker modulation of neuronal activity in the gamma band, since subsequent gamma cycles are occurring at different phases of the carrier activities; and (4) though we induced CCh-evoked network oscillations with a lower concentration of agonist than in earlier studies, in our slices the synchrony of oscillations, and therefore the accuracy of cell firing, can still be higher than that achieved *in vivo*.

Activation of cholinergic and MORs differentially regulates synaptic inhibition mediated by GABAergic cells

Our experiments revealed that during CCh-induced network oscillations in slices the inhibitory transmission of the three types of perisomatic inhibitory cells (and of different other inhibitory cell types) is modulated to a different extent. Application of CCh mimics the high cholinergic tone present during theta-associated behavior with theta-embedded gamma oscillations (Marrosu et al., 1995; Buzsáki et al., 2003). Thus, the demonstrated tuning of different inhibitory circuits, among other effects, might play an important role in switching the hippocampal network from one state to another.

In addition to perisomatic inhibitory cells, a dendrite-targeting GABAergic cell type, the bistratified cells had been suggested to contribute to oscillogenesis, since their firing was found

to be highly modulated by gamma oscillations in *in vivo* recordings (Tukker et al., 2007). However, it is a question whether bistratified cells release transmitter at elevated cholinergic tone and thus participate in the generation of CCh-induced oscillations. To examine this issue directly, we recorded synaptically coupled bistratified cell–pyramidal cell pairs in the CA3 region of the hippocampus. The bath application of 5 μM CCh profoundly reduced the IPSC amplitude measured in these pairs (11.9 ± 7.4% of control amplitude, $n = 5$, $p < 0.001$), showing that in cholinergically induced oscillations in hippocampal slices bistratified cells cannot significantly contribute to the oscillogenesis.

In line with previous findings (Fukudome et al., 2004; Neu et al., 2007), CCh application largely eliminated GABA release from axon terminals of RSBCs, an effect that was mediated via CB_1Rs. These data suggest that IPSCs from RSBCs are not crucial for oscillogenesis, at least in oscillations generated with high cholinergic tone *in vitro*. This suggestion is consistent with the idea that the imprecise input–output function of RSBCs is poorly suited to operate at high frequencies (Hefft and Jonas, 2005; Glickfeld and Scanziani, 2006). The reduction of IPSC amplitude from FSBCs and AACs after CCh application is likely due to the activation of M2 cholinergic receptors located on their presynaptic terminals (Hájos et al., 1998; Fukudome et al., 2004).

Our data obtained from paired recordings showed that MOR activation further reduced the GABA release from FSBCs but did not influence the release of AACs in the presence of CCh. These electrophysiological data agree with the results obtained with immunocytochemistry, showing the presence of MORs at the axon terminals of FSBCs but their lack at the axon endings of AACs (Drake and Milner, 2002).

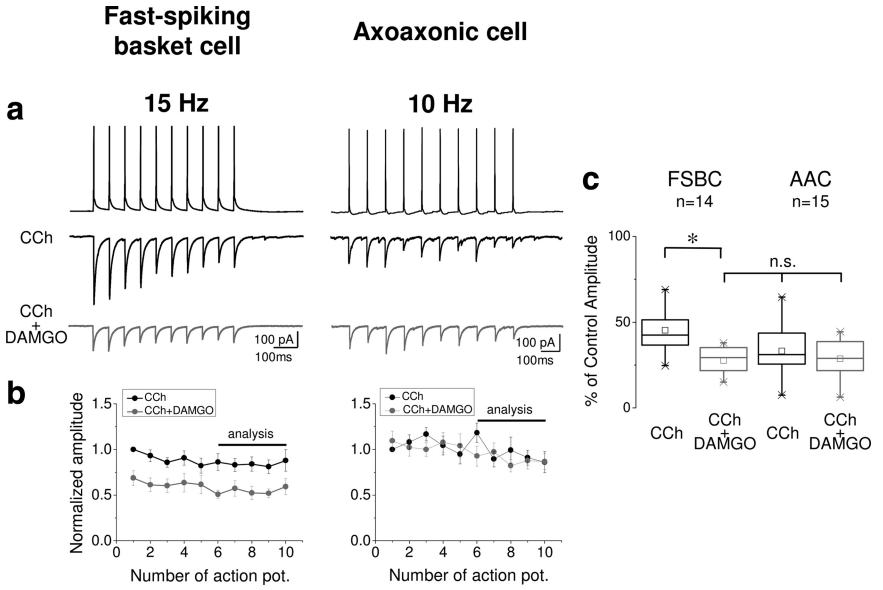

Figure 8. The μ-opiate receptor agonist DAMGO selectively reduces the residual inhibition of FSBCs, but not of AACs, in the presence of CCh. ***a***, ***b***, As demonstrated on the same cell pairs as in Figure 6, DAMGO application did not cause a noticeable decrease in synaptic inhibition of the AAC, but further suppressed the unitary IPSC amplitude of the FSBC. ***c***, While the addition of DAMGO has not significantly reduced further the amplitude of IPSCs in AAC–pyramidal cell pairs (90.4 ± 6.0% of the amplitude in CCh, $n = 15$, $p = 0.15$), there was a significant reduction in the amplitude in FSBC–pyramidal cell pairs (62.3 ± 3.9% of the amplitude in CCh, $n = 14$, $p = 0.001$), decreasing the current amplitudes down to the level of AAC–pyramidal cell pairs ($p = 0.15$).

FSBCs are responsible for most of the perisomatic rhythmic currents generating CCh-induced network oscillations

Since high cholinergic tone mutes GABA release from the axon terminals of RSBCs, the rhythmic discharge of PV-containing perisomatic inhibitory cells remains the only possible source for perisomatic inhibitory currents generating oscillations in local field potentials. This conclusion is supported by recent experiments *in vivo*, in which optically driven PV-containing interneurons in neocortex amplified gamma oscillations (Cardin et al., 2009). Our experiments with DAMGO further differentiated the role of PV-containing FSBCs and AACs in oscillogenesis. The fact that DAMGO potently blocks network oscillation, by selectively reducing GABA release from the axon terminals of FSBCs in the presence of CCh, supports the key role of FSBCs in the generation of rhythmic inhibitory currents that temporally structure the oscillation in CCh-induced synchronous activities in CA3.

The question arises whether DAMGO would be able to suppress the CCh-induced oscillation if the GABA release was normal from the axon terminals of RSBCs (i.e., when the firing of RSBCs would give rise to IPSCs during oscillations). To clarify this issue, we induced oscillations with CCh in hippocampal slices prepared from CB_1R knock-out mice, where CCh does not alter the GABA release of RSBCs (Neu et al., 2007). Comparable to those results obtained in wild-type mice, DAMGO could reduce, or even eliminate the CCh-induced oscillations in slices from these knock-outs (supplemental Fig. 9, available at www.jneurosci.org as supplemental material). This finding further supports our main conclusion that fast-spiking basket cells alone can generate oscillations in the cholinergic model of oscillations, even if the function of RSBCs is intact.

As DAMGO suppressed the oscillation, the pyramidal cell firing and consequently the EPSCs became desynchronized as a result of the elimination of phasic inhibition originating from FSBCs. Thus, DAMGO did not diminish activity in the CA3 network, only let pyramidal cells discharge without rhythmic entrainment (i.e., out of synchrony). This observation suggests that endogenously released opioids might set the level of synchrony and thereby the mode of information processing in the hippocampus. Since dynorphin is present in the mossy terminals of dentate granule cells (Torres-Reveron et al., 2009), which are located adjacent to the MOR-expressing axon terminals of FSBCs, one might speculate that dynorphin release during highly synchronized activities in the dentate gyrus might contribute to the feedforward suppression of oscillations in CA3 (Bragin et al., 1995a,b).

In conclusion, our data indicate that FSBCs represent the most important inhibitory component of the network that generates oscillation in the presence of CCh. Our experiments also revealed a possible mechanism for how opiates interfere with oscillogenesis and thus with cognitive functions (Smith et al., 1962; Braida et al., 1994; Whittington et al., 1998).

References

Atallah BV, Scanziani M (2009) Instantaneous modulation of gamma oscillation frequency by balancing excitation with inhibition. Neuron 62:566–577.

Bragin A, Jandó G, Nádasdy Z, van Landeghem M, Buzsáki G (1995a) Den-

tate EEG spikes and associated interneuronal population bursts in the hippocampal hilar region of the rat. J Neurophysiol 73:1691–1705.
Bragin A, Jandó G, Nádasdy Z, Hetke J, Wise K, Buzsáki G (1995b) Gamma (40–100 Hz) oscillation in the hippocampus of the behaving rat. J Neurosci 15:47–60.
Braida D, Gori E, Sala M (1994) Relationship between morphine and etonitazene-induced working memory impairment and analgesia. Eur J Pharmacol 271:497–504.
Buzsáki G, Buhl DL, Harris KD, Csicsvari J, Czéh B, Morozov A (2003) Hippocampal network patterns of activity in the mouse. Neuroscience 116:201–211.
Cardin JA, Carlén M, Meletis K, Knoblich U, Zhang F, Deisseroth K, Tsai LH, Moore CI (2009) Driving fast-spiking cells induces gamma rhythm and controls sensory responses. Nature 459:663–667.
Cobb SR, Buhl EH, Halasy K, Paulsen O, Somogyi P (1995) Synchronization of neuronal activity in hippocampus by individual GABAergic interneurons. Nature 378:75–78.
Cohen GA, Doze VA, Madison DV (1992) Opioid inhibition of GABA release from presynaptic terminals of rat hippocampal interneurons. Neuron 9:325–335.
Csicsvari J, Jamieson B, Wise KD, Buzsáki G (2003) Mechanisms of gamma oscillations in the hippocampus of the behaving rat. Neuron 37:311–322.
Daw MI, Tricoire L, Erdelyi F, Szabo G, McBain CJ (2009) Asynchronous transmitter release from cholecystokinin-containing inhibitory interneurons is widespread and target-cell independent. J Neurosci 29:11112–11122.
Drake CT, Milner TA (2002) Mu opioid receptors are in discrete hippocampal interneuron subpopulations. Hippocampus 12:119–136.
Fisahn A, Pike FG, Buhl EH, Paulsen O (1998) Cholinergic induction of network oscillations at 40 Hz in the hippocampus in vitro. Nature 394:186–189.
Freund TF, Katona I (2007) Perisomatic inhibition. Neuron 56:33–42.
Fuchs EC, Zivkovic AR, Cunningham MO, Middleton S, Lebeau FE, Bannerman DM, Rozov A, Whittington MA, Traub RD, Rawlins JN, Monyer H (2007) Recruitment of parvalbumin-positive interneurons determines hippocampal function and associated behavior. Neuron 53:591–604.
Fukudome Y, Ohno-Shosaku T, Matsui M, Omori Y, Fukaya M, Tsubokawa H, Taketo MM, Watanabe M, Manabe T, Kano M (2004) Two distinct classes of muscarinic action on hippocampal inhibitory synapses: M2-mediated direct suppression and M1/M3-mediated indirect suppression through endocannabinoid signalling. Eur J Neurosci 19:2682–2692.
Glickfeld LL, Scanziani M (2006) Distinct timing in the activity of cannabinoid-sensitive and cannabinoid-insensitive basket cells. Nat Neurosci 9:807–815.
Glickfeld LL, Atallah BV, Scanziani M (2008) Complementary modulation of somatic inhibition by opioids and cannabinoids. J Neurosci 28:1824–1832.
Gloveli T, Dugladze T, Saha S, Monyer H, Heinemann U, Traub RD, Whittington MA, Buhl EH (2005) Differential involvement of oriens/pyramidale interneurones in hippocampal network oscillations in vitro. J Physiol 562:131–147.
Hájos N, Paulsen O (2009) Network mechanisms of gamma oscillations in the CA3 region of the hippocampus. Neural Netw 22:1113–1119.
Hájos N, Papp EC, Acsády L, Levey AI, Freund TF (1998) Distinct interneuron types express m2 muscarinic receptor immunoreactivity on their dendrites or axon terminals in the hippocampus. Neuroscience 82:355–376.
Hájos N, Pálhalmi J, Mann EO, Németh B, Paulsen O, Freund TF (2004) Spike timing of distinct types of GABAergic interneuron during hippocampal gamma oscillations in vitro. J Neurosci 24:9127–9137.
Hájos N, Ellender TJ, Zemankovics R, Mann EO, Exley R, Cragg SJ, Freund TF, Paulsen O (2009) Maintaining network activity in submerged hippocampal slices: importance of oxygen supply. Eur J Neurosci 29:319–327.
Hefft S, Jonas P (2005) Asynchronous GABA release generates long-lasting inhibition at a hippocampal interneuron-principal neuron synapse. Nat Neurosci 8:1319–1328.
Jenkins SM, Bennett V (2001) Ankyrin-G coordinates assembly of the spectrin-based membrane skeleton, voltage-gated sodium channels, and L1 CAMs at Purkinje neuron initial segments. J Cell Biol 155:739–746.
Klausberger T, Somogyi P (2008) Neuronal diversity and temporal dynamics: the unity of hippocampal circuit operations. Science 321:53–57.
López-Bendito G, Sturgess K, Erdélyi F, Szabó G, Molnár Z, Paulsen O (2004) Preferential origin and layer destination of GAD65-GFP cortical interneurons. Cereb Cortex 14:1122–1133.
Lorincz A, Nusser Z (2008) Cell-type-dependent molecular composition of the axon initial segment. J Neurosci 28:14329–14340.
Maier N, Nimmrich V, Draguhn A (2003) Cellular and network mechanisms underlying spontaneous sharp wave-ripple complexes in mouse hippocampal slices. J Physiol 550:873–887.
Mann EO, Suckling JM, Hajos N, Greenfield SA, Paulsen O (2005) Perisomatic feedback inhibition underlies cholinergically induced fast network oscillations in the rat hippocampus in vitro. Neuron 45:105–117.
Marrosu F, Portas C, Mascia MS, Casu MA, Fà M, Giagheddu M, Imperato A, Gessa GL (1995) Microdialysis measurement of cortical and hippocampal acetylcholine release during sleep-wake cycle in freely moving cats. Brain Res 671:329–332.
Masukawa LM, Prince DA (1982) Enkephalin inhibition of inhibitory input to CA1 and CA3 pyramidal neurons in the hippocampus. Brain Res 249:271–280.
Matthes HW, Maldonado R, Simonin F, Valverde O, Slowe S, Kitchen I, Befort K, Dierich A, Le Meur M, Dollé P, Tzavara E, Hanoune J, Roques BP, Kieffer BL (1996) Loss of morphine-induced analgesia, reward effect and withdrawal symptoms in mice lacking the mu-opioid-receptor gene. Nature 383:819–823.
Meyer AH, Katona I, Blatow M, Rozov A, Monyer H (2002) *In vivo* labeling of parvalbumin-positive interneurons and analysis of electrical coupling in identified neurons. J Neurosci 22:7055–7064.
Miles R, Tóth K, Gulyás AI, Hájos N, Freund TF (1996) Differences between somatic and dendritic inhibition in the hippocampus. Neuron 16:815–823.
Montgomery SM, Buzsáki G (2007) Gamma oscillations dynamically couple hippocampal CA3 and CA1 regions during memory task performance. Proc Natl Acad Sci U S A 104:14495–14500.
Nelson S, Toth L, Sheth B, Sur M (1994) Orientation selectivity of cortical neurons during intracellular blockade of inhibition. Science 265:774–777.
Neu A, Földy C, Soltesz I (2007) Postsynaptic origin of CB1-dependent tonic inhibition of GABA release at cholecystokinin-positive basket cell to pyramidal cell synapses in the CA1 region of the rat hippocampus. J Physiol 578:233–247.
Oren I, Mann EO, Paulsen O, Hájos N (2006) Synaptic currents in anatomically identified CA3 neurons during hippocampal gamma oscillations *in vitro*. J Neurosci 26:9923–9934.
Oren I, Hájos N, Paulsen O (2010) Identification of the current generator underlying cholinergically-induced gamma frequency field potential oscillations in the hippocampal CA3 region. J Physiol 588:785–797.
Paulsen O, Moser EI (1998) A model of hippocampal memory encoding and retrieval: GABAergic control of synaptic plasticity. Trends Neurosci 21:273–278.
Sederberg PB, Kahana MJ, Howard MW, Donner EJ, Madsen JR (2003) Theta and gamma oscillations during encoding predict subsequent recall. J Neurosci 23:10809–10814.
Singer W (1993) Synchronization of cortical activity and its putative role in information processing and learning. Annu Rev Physiol 55:349–374.
Smith GM, Semke CW, Beecher HK (1962) Objective evidence of mental effects of heroin, morphine and placebo in normal subjects. J Pharmacol Exp Ther 136:53–58.
Somogyi P, Smith AD, Nunzi MG, Gorio A, Takagi H, Wu JY (1983) Glutamate decarboxylase immunoreactivity in the hippocampus of the cat. Distribution of immunoreactive terminals with special reference to the axon initial segment of pyramidal neurons. J Neurosci 3:1450–1468.
Steriade M (2006) Grouping of brain rhythms in corticothalamic systems. Neuroscience 137:1087–1106.
Tiitinen H, Sinkkonen J, Reinikainen K, Alho K, Lavikainen J, Näätänen R (1993) Selective attention enhances the auditory 40-hz transient response in humans. Nature 364:59–60.
Torres-Reveron A, Khalid S, Williams TJ, Waters EM, Jacome L, Luine VN, Drake CT, McEwen BS, Milner TA (2009) Hippocampal dynorphin immunoreactivity increases in response to gonadal steroids and is positioned for direct modulation by ovarian steroid receptors. Neuroscience 159:204–216.
Tukker JJ, Fuentealba P, Hartwich K, Somogyi P, Klausberger T (2007) Cell type-specific tuning of hippocampal interneuron firing during gamma oscillations *in vivo*. J Neurosci 27:8184–8189.
Ulbert I, Halgren E, Heit G, Karmos G (2001) Multiple microelectrode-recording system for human intracortical applications. J Neurosci Methods 106:69–79.
Whittington MA, Traub RD, Faulkner HJ, Jefferys JG, Chettiar K (1998) Morphine disrupts long-range synchrony of gamma oscillations in hippocampal slices. Proc Natl Acad Sci U S A 95:5807–5811.